JOURNAL OF GEOPHYSICAL RESEARCH, VOL. 99, NO. B9, PAGES 17,729–17,742, SEPTEMBER 10, 1994

Melting experiments on anhydrous peridotite KLB-1 from 5.0 to 22.5 GPa

Jianzhong Zhang

Center for High Pressure Research and Mineral Physics Institute
State University of New York at Stony Brook

Claude Herzberg[1]

Department of Geological Sciences, Rutgers University, New Brunswick, New Jersey

Abstract. Melting experiments have been performed on anhydrous mantle peridotite KLB-1 at 5 to 22.5 GPa using the multianvil press, with special attention paid to precision and accuracy of temperature and pressure measurement, oxygen fugacity, equilibrium, temperature gradient, and the effects of temperature gradient on the phase diagrams. The new phase diagram reveals complexities in the liquidus and solidus phase relations that were not reported by Takahashi (1986). At no pressure do the liquidus and solidus converge to a common temperature or to a narrow range of temperatures, a result that refutes the conjecture that mantle peridotite formed on the solidus as a partial melt (Herzberg and O'Hara, 1985) or a residual liquid. However, mantle peridotite could have formed as a cotectic liquid because KLB-1 exhibits nearly cotectic liquidus crystallization behavior in garnet plus magnesiowüstite [L + Gt + Mw] from 18 to 22 GPa. The implication is that mantle peridotite may be the product of a large-scale differentiation event and that MgO/SiO_2 for mantle peridotite may have been phase equilibrium controlled by cotectic crystallization in a magma ocean. Fractionation of magnesiowüstite or majorite garnet is inferred at 18 to 22 GPa for a bulk Earth MgO/SiO_2 that is higher or lower than mantle peridotite, respectively. Alternatively, if the Earth formed from materials that were the same in MgO/SiO_2 as mantle peridotite, then the liquidus phase equilibria reported here may be irrelevant or incidental in understanding Earth structure.

Introduction

The liquidus phase relations for mantle peridotite to pressures extending into the lower mantle are important for testing possible magma ocean origins for early Earth history. The solidus phase relations are important because they constrain the compositions of magmas formed on it, and the temperatures of the solidus constrain the conditions of melting and the rheological properties of the mantle. Both kinds of information are contained in the phase diagram for mantle peridotite.

The first estimates of the phase diagram for mantle peridotite in the melting region and at pressures exceeding 10 GPa [*Herzberg*, 1983] were roughly supported by pioneering experimental observations made possible by the multianvil press in Japan [*Takahashi and Scarfe*, 1985; *Takahashi*, 1986; *Takahashi et al.*, 1985; *Ito and Takahashi*, 1987]. Experiments performed on mantle peridotite KLB-1 [*Takahashi*, 1986;] showed that the solidus and liquidus, which differ by ~500°C at 1 atm, appeared to converge at about 15 GPa. At this pressure of apparent convergence, mantle peridotite was observed to be multiply saturated in olivine and garnet [*Takahashi*, 1986; *Ito and Takahashi*, 1987]. But the data were not of sufficiently high resolution to determine if it was also saturated in other crystalline phases, an observation that would have provided strong support for a partial melt [*Herzberg and O'Hara*, 1985] or residual liquid origin for mantle peridotite. The problem of forming mantle peridotite by crystal-liquid differentiation was subsequently examined from the point of view of trace element partitioning [e.g., *Kato et al.*, 1988a, b; *Agee and Walker*, 1988], although trace element tests are ambiguous for mantle peridotite that has experienced subsequent stages of partial melting with garnet in the residuum [*Herzberg and Gasparik*, 1991].

These early high-pressure melting studies have been reproduced in a qualitative manner in that there is overall agreement with the general topological characteristics of the phase diagram [*Herzberg et al.*, 1990] (also this work). However, a number of melting studies on mantle peridotite have revealed complexities that were not reported by *Takahashi* [1986]. These are the observation of magnesiowüstite saturation at 16.5 GPa [*McFarlane et al.*, 1991], disagreements in the pressure at which orthopyroxene remains a crystallizing phase [*Takahashi*, 1986; *Takahashi et al.*, 1993; *Herzberg*, 1992; *Canil*, 1992], and solidus temperature determinations that are consistently higher [*Herzberg et al.*, 1990] than those reported earlier. For these reasons an attempt has been made to reproduce the phase diagram for anhydrous peridotite KLB-1 published by *Takahashi* [1986, Figure 13],

[1]Also at Center for High Pressure Research and Mineral Physics Institute, State University of New York at Stony Brook.

Paper number 94JB01406.
0148-0227/94/94JB-01406$05.00

Table 1. Compositions of Peridotite KLB-1

	Takahashi [1986]	*Herzberg et al.* [1990]	KLB-1 Liquid*
SiO_2	44.48	44.30	45.55 (0.94)
TiO_2	0.16	0.12	0.12 (0.03)
Al_2O_3	3.59	3.54	3.50 (0.49)
FeO	8.10	8.59	9.04 (0.77)
MnO	0.12	0.14	0.14 (0.03)
MgO	39.22	39.50	36.63 (1.32)
CaO	3.44	3.03	3.26 (0.43)
Na_2O	0.30	0.30	0.33 (0.08)
K_2O	0.02	0.01	...
Cr_2O_3	0.31	...	0.38 (0.04)
NiO	0.25	...	0.21 (0.03)

In weight percent.

*KLB-1 liquid is the average of 148 electron microprobe analyses above the liquidii at 18, 20, and 21.7 GPa for experiments KLB1-10, KLB1-15, and KLB1-11, respectively. Numbers in parentheses are 1 standard deviation.

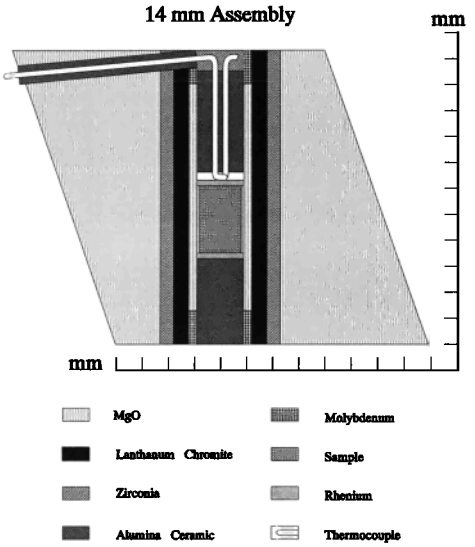

Figure 1. Construction of the 14-mm assembly used in experiments below 10 GPa. Dimensions of the essential parts are as follows: lanthanum chromite heater length = 11.3 mm, ID = 2.4 mm, OD = 4.6 mm, thermocouple ceramic = 3.9 mm, and capsule length = 3.0 mm.

and the results are reported in this paper. Building on *Takahashi*'s [1986] contribution, we have succeeded in obtaining a greatly improved understanding of the liquidus and solidus phase relations, in addition to a highly precise calibration of the temperatures and pressures at which they occur.

Experimental Method

Samples of peridotite KLB-1 were kindly donated by E. Takahashi, and several experiments were reported at 14 GPa [*Herzberg et al.*, 1990]. Chemical analyses of KLB-1 reported by *Takahashi* [1986] are given in Table 1 and are in fairly good agreement with analyses determined by direct current plasma (DCP) emission spectroscopy at Rutgers [*Herzberg et al.*, 1990]. All experiments were conducted with the multianvil apparatus at Stony Brook. Detailed descriptions of the press, the 10-mm sample assemblies, and the experimental methods have been published [*Gasparik*, 1989, 1990; *Herzberg et al.*, 1990; *Liebermann and Wang*, 1992].

The high-pressure assemblies were configured with W3%Re versus W25%Re thermocouples positioned along the axis of the lanthanum chromite heaters as described previously [*Gasparik*, 1989; *Herzberg et al.*, 1990]. Assemblies with 10-mm octahedral edge lengths were used at pressures of ≥15 GPa in conjunction with tungsten carbide cubic anvils with corners honed down to triangular faces 4 mm or 5 mm in edge length. Assemblies with 14-mm edge lengths were used at pressures of <10 GPa, together with 8-mm tungsten carbide edge lengths. This 14/8-mm system is basically a scaled-up version of the 10/5 system that has been described previously [*Gasparik*, 1989; *Herzberg et al.*, 1990], and its construction is shown in Figure 1.

The pressure calibration curves used in this study for the 10/4 and 10/5 systems are the ones reported by *Gasparik* [1989, 1990]. For the 14/8-mm assembly the pressure was calibrated against several high-temperature transformations: coesite-stishovite at 2000°C and 11.3 GPa [*Zhang et al.*, 1993], quartz-coesite at 1600°C and 3.74 GPa [*Mirwald and Massonne*, 1980], and garnet-perovskite in the system $CaGeO_3$ at 1000°C and 6.1 GPa [*Susaki et al.*, 1985]. The resulting pressure calibration curve for the 14/8-mm system is shown in Figure 2.

KLB-1 powder was loaded into unwelded rhenium foil. The assemblies containing the sample, thermocouple, lanthanum chromite heater, and spacers were constructed and then fired at 1000°C in an argon atmosphere for 1 hour prior to running to expel all water. The oxygen fugacity of this system is slightly more oxidizing than the iron-wüstite buffer, and this is discussed below. The assembly was pressurized first, then heated to the desired temperature. About 15 to 20 min of heating was required to reach the target temperature, which was then maintained for a run duration of 2 to 12 min (Table 2), and the experiment was terminated by cutting off the power. A 10^5-Pa thermocouple emf-temperature relation was used with no corrections made for pressure. These emf readings are included in Table 2 in the event that the effect of pressure on thermocouple emf

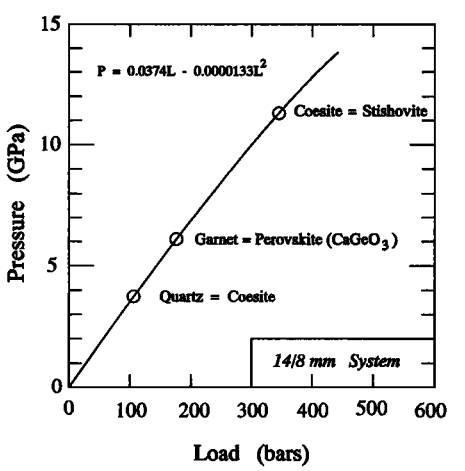

Figure 2. A pressure calibration at high temperatures for the 14/8-mm system.

Table 2. Experimental Results

Run[a]	emf,[b] mV	Temperature,[c] °C	Oil Pressure, bars	Assembly[d]	Sample Pressure, GPa	Time, min	Phase Assemblage[e]
26.1809	29.60	1650 (4)	140	A	5.0	10	[Ol, Gt, Cpx]*
27.1862	30.58	1700 (4)	140	A	5.0	8	[Ol, Gt, Cpx]*
25.1788	31.32	1750 (1)	140	A	5.0	10	L, Ol, Opx, Gt*, Cpx [Ol, Gt, Cpx]
34.1893	33.15	1855 (5)	140	A	5.0	6	L, Ol*, Opx, Gt, Cpx [Ol, Gt, Cpx]
28.1856	33.85	1900 (1)	140	A	5.0	8	L, Ol*, Opx, Gt, Cpx [Ol, Gt, Cpx]
29.1829	34.58	1950 (2)	140	A	5.0	8	L*, Ol, Opx, Gt, Cpx [Ol, Gt, Cpx]
35.1879	34.59	1950 (1)	214	A	7.4	8	L, Ol*, Gt, Opx, Cpx [Ol, Gt, Cpx]
18.1750	32.93	1850 (2)	290	A	9.7	6	[Ol, Gt, Cpx]*
19.1749	33.74	1900 (1)	290	A	9.7	8	[Ol, Gt, Cpx]*
23.1768	34.43	1950 (5)	290	A	9.7	8	[Ol, Gt, Cpx]*
24.1789	35.18	2000 (1)	290	A	9.7	8	L, Ol, Gt*, Cpx [Ol, Gt, Cpx]
30.1854	36.00	2050 (1)	290	A	9.7	8	L, Ol*, Gt, Cpx [Ol, Gt, Cpx]
31.1831	36.78	2110 (5)	290	A	9.7	6	L*, Ol, Gt, Cpx [Ol, Gt, Cpx]
37.1293 (Fe^0 added)	36.62	2080 (1)	305	B	14.0	2	L, Ol + Gt + Fe^0*, Cpx [Ol, Gt, Cpx, Fe^0]
38.1309	36.62	2080 (3)	305	B	14.0	3	L, Gt, Ol*, Cpx [Ol, Gt, Cpx]
16.1730	36.00	2060 (1)	386	B	15.0	5	L, Gt, Ol*, Cpx [Ol, Gt, Cpx]
7.1610	36.54	2100 (4)	386	B	15.0	4	L, Gt, AnhyB, Ol* [Ol, Gt]
39.2044	37.00	2135 (2)	430	B	15.5	2	L, Gt, AnhyB, Ol*, β [β, Gt]
20.1756	37.00	2135 (2)	430	B	15.5	6	L, Gt, AnhyB, Ol*, β [β, Gt]
40.2076	37.00	2135 (5)	430	B	15.5	12	L, Gt, AnhyB, Ol*, β [β, Gt]
32.1823	36.10	2065 (1)	500	B	16.0	8	[β, Gt]*
8.1615	37.03	2135 (1)	500	B	16.0	4	L, Gt, AnhyB, β* [β, Gt]
9.1693	37.63	2185 (3)	420	C	17.0	5	L, Gt, AnhyB, β* [β, Gt]
22.1775	36.90	2125 (1)	440	C	17.5	8	Gt, Mw, β [β, Gt]*
10.1694	37.75	2195 (5)	463	C	18.0	2	L, Gt, Mw, β* [β, Gt]
12.1719	37.88	2205 (1)	510	C	19.0	4	L, Gt, Mw, β* [β, Gt, Mw]
33.1835	36.90	2115 (8)	560	C	20.0	8	[β, Gt, Mw]*
13.1735	37.20	2150 (4)	560	C	20.0	2	Gt, Mw, β* [β, Gt, Mw]
15.1732	38.00	2215 (2)	560	C	20.0	4	L, Gt, Mw, β* [β, Gt, Mw]
21.1765	38.03	2220 (1)	590	C	20.5	6	L, Gt, Mw, β*, CaPv [β, τ, Gt, Mw, CaPv]
14.1706	37.92	2210 (3)	615	C	21.0	4	L, Gt, Mw, τ, CaPv [τ, Gt, Mw, CaPv]
11.1698	38.27	2240 (1)	680	C	21.7	5	L, Gt + Mw*, τ + CaPv [τ, Gt, Mw, CaPv]
17.1743	37.00	2135 (5)	800	C	22.5	2	L, Mw, MgPv, CaPv [Mw, MgPv, CaPv]*
36.1909	39.85	2375 (5)	800	C	22.5	4	L, Mw*, MgPv, CaPv [Mw, MgPv, CaPv]

Experiments KLB1-1 to KLB1-6 were reported by *Herzberg et al.* [1990].
[a]Runs are read as follows: run 26.1809 is 26th experiment on KLB-1, Stony Brook run 1809.
[b]The emf is nominal pressure-uncorrected emf for W3 %Re versus W25 %Re thermocouples.
[c]Values are read as follows: temperature fluctuation: 1650 (4) = 1650° ± 4°C.
[d]Assemblies are A = 14/8 mm, B = 10/5 mm, and C = 10/4 mm.
[e]Asterisk indicates phase assemblage at T (see text). Square brackets indicate phases observed immediately below the solidus.

becomes better known; however, the discussion below indicates the pressure derivative of the thermocouple temperature may be about -5°C GPa^{-1}.

The phases were identified by energy dispersive analysis of polished sections utilizing the backscatter scanning electron microscope (SEM) unit contained in the Rutgers JEOL 3600 electron microprobe. The experimental results are listed in Table 2. Fully quantitative wavelength dispersive analyses are being acquired; some are reported here, but a comprehensive database for all coexisting crystalline and liquid phases will be reported in a forthcoming paper. Throughout this paper, liquid is identified as a complex intergrowth of phases quenched from liquid. Polymorphs of $(Mg, Fe)_2SiO_4$ at $\geq$15 GPa were identified according to olivine (α), modified spinel (β), and spinel (τ) by their Raman spectra [*McMillan and Akaogi*, 1987].

There now exist many published descriptions of the temperature gradient in 10-mm assemblies [*Gasparik*, 1989; *Herzberg et al.*, 1990; *Presnall and Gasparik*, 1990; *Herzberg*, 1992]. The temperature gradient in 14-mm assemblies has been determined by mapping the isobaric shifts in the solidus with increasing temperature, and the results are shown in Figure 3. The temperature varies by no more than about 50°C in an area of 1 mm × 1 mm nearest the hot spot, a gradient that is considerably less than that which has been observed in 10-mm assemblies [*Gasparik*, 1989; *Herzberg et al.*, 1990; *Presnall and Gasparik*, 1990]. Figures 4 and 5 show that the temperature gradient within the axial portion of the 5-GPa charges must be sufficiently small to retard melt migration because a substantial amount of intercumulus liquid can be seen surrounding the olivine crystals. A magnified view of the 1950°C experiment (Figure 5) shows the intercumulus liquid in more detail, in addition to the kind of olivine morphologies that are observed. Olivine C crystallographic axes parallel the temperature gradient [*Herzberg et al.*, 1990], and Figure 5 shows the development of euhedral ($h0l$) or ($0kl$) crystallographic faces in the direction of the hot spot. Olivine crystals facing the cold direction are distinctly anhedral with embayments containing liquid. The temperature gradient is therefore sufficiently large on a scale of 100 μm that precipitation occurs on the hot ends and dissolution on the cold ends of individual crystals, a process that was also documented in a reversal experiment on garnet crystals [*Herzberg et al.*, 1990]. Inspection of Figure 4 shows

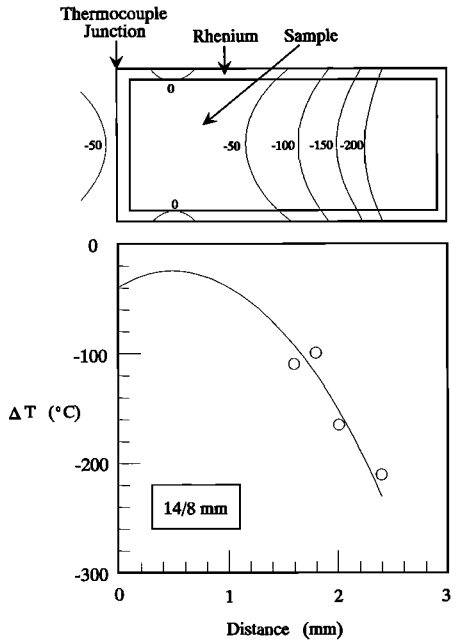

Figure 3. Temperature gradient in the 14-mm assembly determined by shifts in the solidus for KLB-1 with increasing temperature. (Top) A slice through a horizontally positioned cylinder of sample contained in rhenium is shown. (Bottom) The solidus position is along the axis of the sample; measurements of the distance of the solidus from the thermocouple junction are given (circles). The gradient around the hot spot is constrained by the 50°C solidus brackets at 5 and 10 GPa.

that the radial temperature gradients are actually larger than those shown in Figure 3 at elevated temperatures. Although shifts in the liquidus generally follow shifts in the solidus along the axial portions of the charge, there is a substantial temperature gradient next to the capsule wall as shown by the extensive amount of liquid adjacent to it.

There are both advantages and difficulties in obtaining phase equilibrium information in a temperature gradient. The advantage is that an isobaric phase diagram can often be observed in a single experiment; in melting experiments the important features to observe are the liquidus and solidus mineralogies and the crystallization sequence between them [*Herzberg et al.*, 1990; *Herzberg*, 1992]. For example, in experiment KLB1-34 listed in Table 2, the following phase assemblages are observed down the temperature gradient at 5 GPa: [L], [L + Ol]*, [L + Ol + Opx], [L + Ol + Opx + Gt], [L + Ol + Opx + Gt + Cpx], and [Ol + Gt + Cpx]; the shorthand notation which describes this crystallization sequence in Table 2 is L, Ol, Opx, Gt, Cpx [Ol, Gt, Cpx], with phases in square brackets indicating the phases which are observed immediately below the solidus (symbols are defined in the caption for Figure 6). The thermocouple emf is valid at only one point along this temperature gradient, and this can pose a problem in determining which of these phase assemblages the thermocouple emf is valid for. In most experiments the hot spot can be observed, and it is usually located about 0.5 ± 0.2 mm from the thermocouple junction, a distance that is common to both 10- and 14-mm assemblies. Since the temperature gradient is approximately symmetrical on each side of the hot spot, the phase assemblage that is stable for the nominal temperature is the one that is observed 0.5 ± 0.2 mm from the hot spot toward the cold end of the capsule. For KLB1-34 this is [L + Ol], indicated by the asterisk in Table 2 next to it (i.e., [L + Ol]*).

Another difficulty in working with a temperature gradient is liquid migration toward the hot spot by a solution and precipitation process [*Lesher and Walker*, 1988; *Herzberg et al.*, 1990]. When there is a substantial amount liquid near the hot spot, there should be no change in the nature of the liquidus phase mineralogy [*Lesher and Walker*, 1988] and the crystallization sequence [*Herzberg*, 1992]. However, when the melt fraction in the charge is very small and confined to pockets that are within ~10–20 μm of the capsule wall, any of the phase assemblages from the liquidus to the solidus can be observed. We are now in the process of compiling electron microprobe data on the quenched liquid portions of the charges, some of which are reported below. However, the data obtained demonstrate that the liquid compositions are largely mixtures of the bulk KLB-1 composition and liquid from the colder portions of the charge, modified slightly by liquidus phase fractionation effects that occur during melting.

Presnall and Walter [1993] have observed complexities in the crystallization sequence for forsterite Mg_2SiO_4 at 14 GPa that arise from variable run durations. In a 3-min experiment they observed the following phases down the temperature gradient: [L], [L + periclase], [L + periclase + forsterite], and [forsterite]. This is very different from their 43-min experiment, which shows [L] followed by monomineralic bands of [forsterite], [periclase], and [forsterite]. *Presnall and Walter* [1993, p. 19,780] were thus perplexed by the dilemma that "if run durations are held to very short times (1 or 2 min) . . . chemical equilibrium cannot be assured. On the other hand, if run durations are extended in order to assure equilibrium, then the phase assemblages observed are prone to misinterpretation." *Presnall and Walter* [1993] are apparently unaware that equilibrium was determined to occur in a 3-min experiment at 2200°C from a reversal performed on pyrope and grossular seeds in a peridotite liquid [*Herzberg et al.*, 1990]. Electron microprobe results showed that the composition of the liquidus majorite garnet was controlled by precipitation from the liquid and dissolution of grossular and pyrope seeds. Backscatter SEM images of pyrope seeds in this experiment clearly showed the precipitation of majorite at the hot side and dissolution of pyrope at the cold side. Simultaneous precipitation and solution of olivine also occurs at 1950°C and 5 GPa within 8 min (Figure 5). We concur with *Walker and Agee* [1989] that because of dissolution and reprecipitation in a temperature gradient, it is "difficult to imagine a process more ideally suited for giving well-equilibrated crystals and physically separated liquid" [*Walker and Agee*, 1989, p. 57]. Electron microprobe results also demonstrate a remarkable level of chemical homogeneity for all phases except garnet. Backscatter SEM images of garnets in Figures 7 to 12 reveal crystals that are homogeneous, but crystals that also show some zonation. This problem was examined in great detail previously [*Herzberg et al.*, 1990], and it was shown that most of this variability is small and occurs from CaO and Al_2O_3 which vary no more than about 1 wt% absolute from core to rim.

The most serious concern of *Presnall and Walter* [1993] is that there may be a misinterpretation of the liquidus phase

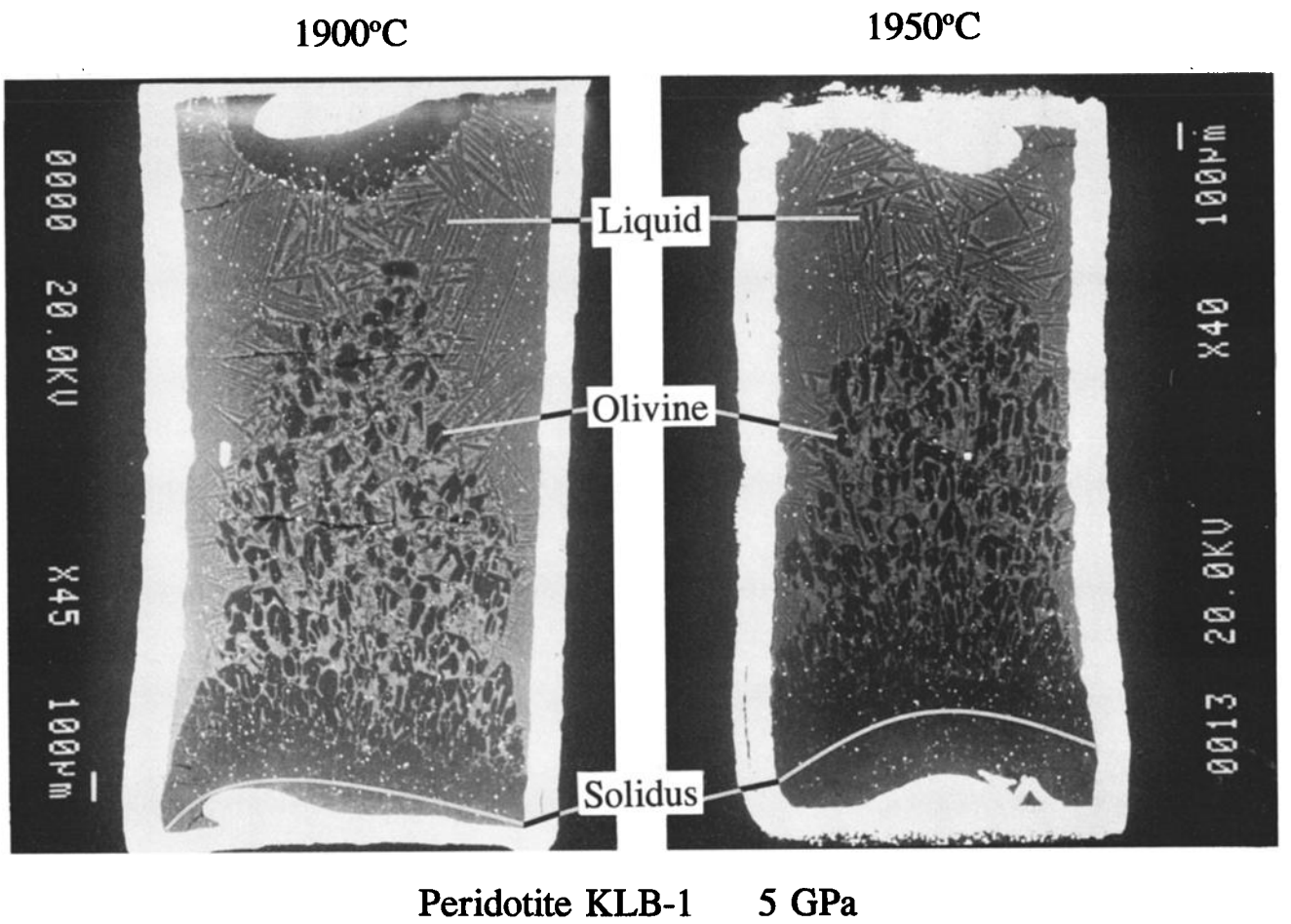

Figure 4. Backscatter SEM photomicrographs of two experiments at 5 GPa in which 14-mm size assemblies were used. The liquidus temperature is bracketed between 1900° and 1950°C (KLB1-28 and KLB1-29). Note the temperature gradient nearest the walls of the container. "Liquid" refers to quench phases formed from liquid.

and crystallization sequence for long-duration experiments in a temperature gradient. This was based on a comparison of their discrepant 3- and 43-min results described above. But our experiments are usually confined to run durations of 3 to 8 min, and within this restricted range of run times we have observed no contradictory results. This is illustrated particularly well by the set of three experiments on KLB-1 at 15.5 GPa and 2135°C (Table 2), in which the run durations were 2, 6, and 12 min. The results for all three runs are identical; L, Gt, AnhyB, Ol, β, [β, Gt]. The only discernable effect of time was to increase the crystal size of anhydrous B phase. We therefore think that the concerns of *Presnall and Walter* [1993] stem from their problematical 43-min experiment, and for 3- to 8-min run durations that are appropriate for the attainment of chemical equilibrium, there is little risk of the misidentification of the crystallization sequence.

Precision in the measurement of pressure is ±0.25 GPa, a result that is discussed in detail below. The experiments at 5 and 9.7 GPa illustrate the high level of precision that can be obtained in the measurement of temperature (Figure 4). In particular, the liquidus and solidus temperatures for KLB-1 have been bracketed between experiments that differ by only 50°C. Temperature accuracy is more problematical because the effect of pressure on thermocouple emf is not known. It is worth noting, however, that the melting temperature of $MgSiO_3$ perovskite at 22 GPa was determined by *Zerr and Boehler* [1993] using a CO_2 laser-heated diamond cell to be 2727°C with a reported accuracy of ±50°C. *Ito and Katsura* [1992] report melting of $MgSiO_3$ at 2450°C and 22 GPa using tungsten rhenium thermocouples, and *Gasparik* [1990] estimated it at 2600°C and 22.5 GPa, a temperature difference that arises from different thermocouple configurations (see below). If the error quoted by *Zerr and Boehler* [1993] is realistic, then it can be determined that tungsten rhenium thermocouples read about 100°C too low at 22 GPa, resulting in a pressure derivative of the thermocouple temperature of approximately -5°C GPa^{-1}.

Another difficulty in working with a temperature gradient can be estimating the temperature of the solidus in experiments for which the melt fraction is substantial. Of the photomicrographs shown in Figures 4–5 and 7–14, examples of the solidus can be seen in Figures 4, 9, and 13. At pressures less than 15 GPa the solidus is easily identified by the observation of clinopyroxene, and the assemblage [L + Ol + Gt + Cpx] is restricted to a very narrow temperature interval of ~10°C. At 15.5 GPa the assemblage [L + β + Gt] is stable over a temperature interval of about 75°C, and the solidus is defined by crystalline phases that are highest in FeO/MgO because FeO partitions preferrentially into the liquid phase. Changes in FeO can be seen in the grey scaling

Figure 5. Magnified view of experiment at 1950°C and 5 GPa (KLB1-29) showing euhedral olivine crystals facing the hot direction of the temperature gradient. Olivine crystals that face the cold direction are dissolved as seen by embayments filled with liquid.

in Figure 9, and in experiments like these, color-coded chemical maps generated with the electron probe are the best way to observe the solidus. Experiments which contain no melt phase anywhere in the charge remain the most unambiguous way of bracketing the solidus (Table 2; Figure 6).

Experimental Results

Phase Equilibria

The experimental results listed in Table 2 are shown in Figure 6, a new phase diagram for anhydrous peridotite KLB-1. At 5 and 7.4 GPa, orthopyroxene does not occur immediately below the solidus [Ol + Gt + Cpx], but it is observed in the melting interval (Figure 6). This occurs because of the incongruent melting relation Ol + Cpx + Gt = Opx + L that has been observed over a pressure range of 2 to 12 GPa [*Davis*, 1964; *O'Hara and Yoder*, 1967; *Herzberg et al.*, 1990; *Herzberg*, 1992; *Bertka and Holloway*, 1993]. At pressures greater than or equal to 9.7 GPa, orthopyroxene is completely absent for the KLB-1 composition, and this is caused by a contraction of the orthopyroxene liquidus crystallization field [*Herzberg et al.*, 1990]. Our results are similar to those of *Canil* [1992], who documented orthopyroxene in the melting interval at 5 and 6.5 GPa for a peridotite composition similar to KLB-1. However, they differ from the results of *Takahashi* [1986] and *Takahashi et al.* [1993], who observed orthopyroxene in the melting interval only at pressures less than 3.5 GPa. These differences are important because many Munro-type komatiites were likely to have been in equilibrium with harzburgite (Ol + Opx) [*Herzberg*, 1992], and our results show that orthopyroxene can participate in melting to pressures somewhere between 7.4 and 9.7 GPa.

At 14 GPa there is a change in the liquidus mineralogy from olivine below to garnet above, and there is multiple saturation in both at this pressure (Figures 6 and 7). Most of the 14-GPa experiments shown in Figure 6 are those reported earlier (by *Herzberg et al.*, [1990] for KLB1-1 to KLB1-6) in which molybdenum capsules were used. These results are reproduced here using rhenium capsules, and the runs were made with and without metallic iron (KLB1-37 and KLB1-38). In the absence of Fe^0, the liquidus phase at 14 GPa is garnet, and olivine appears several degrees below, indicating that KLB-1 is almost multiply saturated in garnet and olivine [L + Gt + Ol]. The effect of adding Fe^0 is to slightly expand the crystallization field of olivine at the expense of garnet, and KLB-1 is multiply saturated in both olivine and garnet [L + Ol + Gt + Fe^0] at 14 GPa (Figure 7). Electron microprobe results of these two experiments are listed in Table 3. Addition of metallic Fe has the effect of increasing the FeO content of all phases, but the partition coefficients for FeO and MgO among liquid, olivine, and garnet are virtually identical. If the oxygen fugacity of the experiment without Fe^0 was substantially greater, then it would be expected that the stabilization of Fe^{3+} would reduce the amount of Fe^{2+} available to olivine, resulting in a reduction in $D_{FeO}^{Ol/L}$, but this is not observed. It is concluded that the oxygen fugacity of the assemblies used with rhenium capsules is only slightly more oxidizing than the iron-wüstite buffer. Use of molybdenum capsules extracts metallic iron from KLB-1 at 14 GPa [*Herzberg et al.*, 1990], demonstrating that it provides a more reducing environment.

In Figure 8 it can be seen that garnet is the liquidus phase at 15 GPa [L + Gt], and it is joined by olivine several tens of degrees down the temperature gradient [L + Gt + Ol]; the crystallization sequence for this experiment (KLB1-16) is L, Gt, Ol, Cpx [Ol, Gt, Cpx]. In another 15-GPa experiment (KLB1-7), minor amounts of anhydrous B were observed, a dense phase with the stoichiometry $Mg_{14}Si_5O_{24}$ [*Finger et al.*, 1989; *Herzberg et al.*, 1990; *Presnall and Gasparik*, 1990]. These two 15-GPa experiments are the only inconsistent runs in the 40 experiments that were done on KLB-1, indicating a precision in pressure measurement that is well within ±0.25 GPa. It is our experience that inconsistent runs like KLB1-7 can usually be avoided and that they are largely the result of inconsistencies that arise from the construction of the high-pressure assembly.

At 15.5 GPa, liquidus garnet is joined by phase anhydrous B (Figures 9 and 10). The crystallization sequence is [L], [L + Gt], [L + Gt + AnhyB], [L + Gt + Ol], [L + Gt + β], [β + Gt]. Anhydrous B is restricted in its distribution to the hot side of olivine in the temperature gradient (Figure 10), demonstrating that it forms by incongruent melting of olivine [e.g., *Herzberg et al.*, 1990]. The three experiments con-

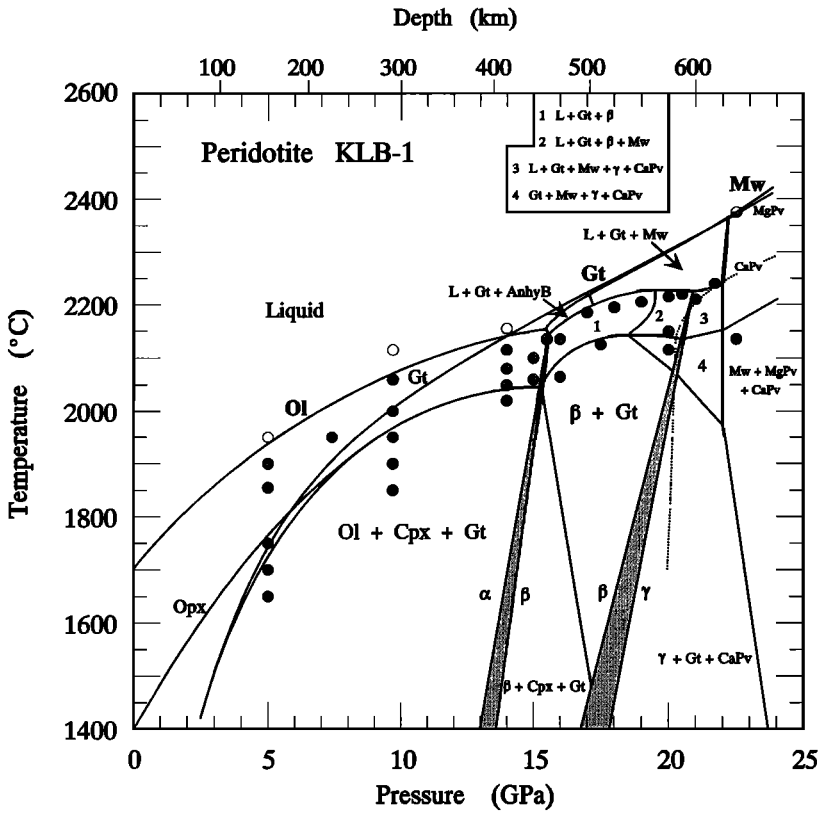

Figure 6. Phase diagram for anhydrous peridotite KLB-1: all crystalline (solid circles), crystals plus liquid (cross-hatched circles), all liquid (open circles), and precise liquidus determination at 2375°C and 22.5 GPa (half open and half cross-hatched circle). Stability of Opx at 1 atm is from *Shimazaki and Takahashi* [1993]. The boundary τ = Mw + MgPv is positioned at 1400°C from *Ito and Takahashi* [1989]. The α-β and β-τ transitions at 1400°C are from *Katsura and Ito* [1989]. The dotted line labeled CaPv positions the stability of calcium silicate perovskite to the right of it, and the positive dT/dP is based on the results of *Irifune and Ringwood* [1987]. Symbols are defined as follows: L, liquid; Ol, olivine; Opx, orthopyroxene; Cpx, clinopyroxene; Gt, garnet; AnhyB, anhydrous B; Mw, magnesiowüstite; MgPv, magnesium silicate perovskite; CaPv, calcium silicate perovskite; α, olivine; β, modified spinel (Mg, Fe)$_2$SiO$_4$; and τ, spinel (Mg, Fe)$_2$SiO$_4$. Experimental results at 14 GPa are from *Herzberg et al.* [1990] and this work (Table 2).

ducted at 2135°C and 15.5 GPa (Table 2) were designed to test both the effect of run duration on the crystallization sequence, as discussed above, and the level of reproducibility that can be achieved. We intentionally choose 15.5 GPa because it is at this pressure that the largest number of important phase changes exists (Figure 6), and therefore there is the greatest risk of obtaining discrepant results. However, we were able to reproduce the same experimental result every time (Table 2). Indeed, the 2- and 6-min experiments at 15.5 GPa are so similar that to the uninformed observer, they could be mistaken for serial sections of the same experiment. The 12-min run is also very similar but shows some grain coarsening of phase anhydrous B.

The 15.5-GPa experiments are special because both olivine (α) and modified spinel (β) are present in the melting interval (Figure 9). Their restricted distribution also demonstrates that the α-β transformation at these temperatures is very sharp. The olivine–modified spinel boundary shown in Figure 6 is an interpolation of our 15.5-GPa experiments with the 1400°C bracket of *Katsura and Ito* [1989]. Extrapolation of the *Katsura and Ito* [1989] α-β transformation to temperatures in the melting range creates a boundary that is indistinguishable from ours and fully supports the interpretation of *Katsura and Ito* [1989] that the loop becomes very narrow at high temperatures. However, *Ito and Takahashi* [1987] reported the α-β transformation at 16 to 17 GPa at solidus temperatures, a difference that is not understood. By and large, there is a great deal of consistency in the pressure calibration scales used in the two laboratories, in addition to a high level of precision in the generation and measurement of pressure.

At 16 and 17 GPa, anhydrous B is found to the hot side of modified spinel, demonstrating that it forms by incongruent melting of modified spinel [*Herzberg et al.*, 1990]. Anhydrous B is also limited in its stability to the 15.5- to 17-GPa range. *Kato and Kumazawa* [1986] and *Ito and Takahashi* [1987] reported it at 20 GPa and erroneously identified it as hydrous phase B; this difference in pressure is probably an artifact of differences in the pressure calibration scales that were used.

Experiments conducted at 18 to 21 GPa demonstrate that garnet is the liquidus phase, but it is joined by magnesiowüstite a few degrees down the temperature gradient. The 20-GPa experiment shown in Figure 11 is fairly representa-

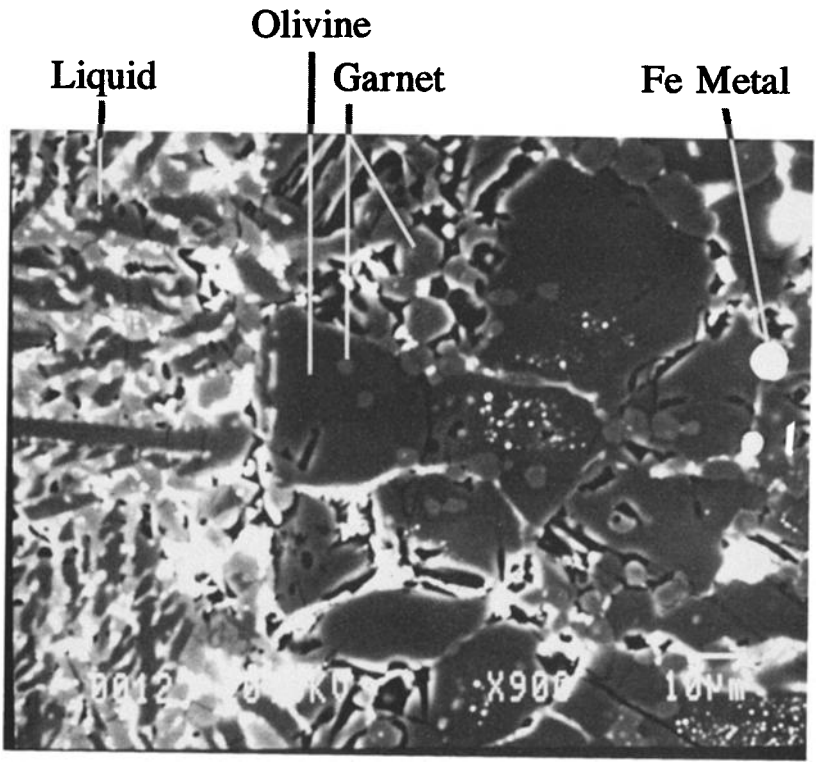

Figure 7. Backscatter SEM photomicrograph of the liquidus portion of a 14-GPa experiment (KLB1-37) run at a nominal temperature of 2080°C, showing multiple saturation in olivine and garnet [L + Ol + Gt] in the presence of metallic iron Fe°.

tive of the others in this wide pressure range. At 21.7 GPa there is multiple saturation in both garnet and magnesiowüstite [L + Gt + Mw], and this is shown in Figure 12. A larger portion of the 21.7-GPa experiment is shown in Figure 13, demonstrating the extensive temperature interval at which garnet and magnesiowüstite coexist with liquid. At 22.5 GPa the liquidus phase is magnesiowüstite, which is joined by magnesium silicate perovskite several degrees down the temperature gradient (Figure 14). Although the effect of pressure is to increase the stability of magnesiowüstite at the expense of garnet and magnesium perovskite, as a first approximation KLB-1 is nearly multiply saturated in garnet plus magnesiowüstite [L + Gt + Mw] and magnesium perovskite plus magnesiowüstite [L + MgPv + Mw] over a pressure range that extends from 18 to 22.5 GPa.

At 18 GPa the distribution of magnesiowüstite is restricted, and the crystallization sequence is [L], [L + Gt], [L + Gt + Mw], [L + Gt + β], [Gt + β]; this demonstrates that magnesiowüstite is formed by incongruent melting of modified spinel, similar to anhydrous B. However, at 19 to 21.7 GPa, magnesiowüstite is observed with both β and τ along and below the solidus. We also observe a very sharp transformation of β to τ, and the boundary shown in Figure 6 is an interpolation of our data with the 1400°C bracket of

Table 3. Compositions of Liquidus Phases in Fe°-Bearing and Fe°-Free Experiments at 14 GPa

	KLB1-38 (Fe° free)			KLB1-37 (Fe° bearing)		
	Olivine	Garnet	Liquid	Olivine	Garnet	Liquid
SiO_2	41.78 (0.38)	49.99 (0.51)	45.76 (0.49)	41.63 (0.43)	50.90 (0.89)	42.79 (0.46)
Al_2O_3	0.16 (0.01)	12.74 (0.81)	3.35 (0.16)	0.19 (0.02)	12.31 (1.62)	3.68 (0.32)
FeO	4.82 (0.14)	3.84 (0.26)	9.63 (0.23)	6.84 (0.42)	5.20 (0.42)	14.09 (0.43)
MgO	52.11 (0.45)	29.44 (0.50)	35.05 (0.70)	51.71 (0.53)	29.19 (0.63)	35.13 (1.04)
CaO	0.12 (0.01)	2.66 (0.41)	3.71 (0.23)	0.12 (0.02)	2.57 (0.58)	3.06 (0.23)
$D_{MgO}^{Ol/L}$	1.487 ± 0.032			1.472 ± 0.046		
$D_{FeO}^{Ol/L}$	0.500 ± 0.019			0.485 ± 0.033		
$D_{MgO}^{Gt/L}$		0.840 ± 0.022			0.831 ± 0.030	
$D_{FeO}^{Gt/L}$		0.399 ± 0.029			0.369 ± 0.032	

Values in parentheses represent 1 standard deviation from multiple analyses and are propagated to the error in D; $D_{MgO}^{\alpha/\beta} = MgO_\alpha/MgO_\beta$.

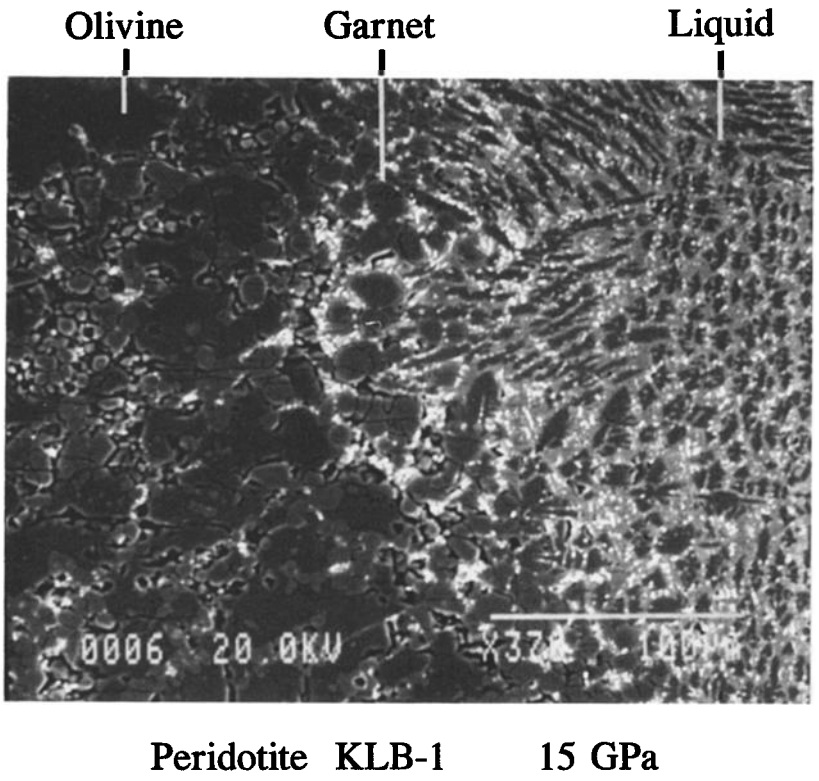

Figure 8. Backscatter SEM photomicrograph of the liquidus portion of a 15-GPa experiment (KLB1-16) run at a nominal temperature of 2060°C. Garnet is the liquidus phase.

Katsura and Ito [1989]. The β-τ transition must be considerably less than 0.5 GPa in width, which is narrower than the 1-GPa transition predicted by *Katsura and Ito* [1989] at melting temperatures. Spinel (τ) is also present in the melting interval at 20.5 to 21.7 GPa, whereas it was reported as unstable at these conditions in experiments on a peridotite of similar composition [*Ito and Takahashi*, 1987].

At 2200°C the transformation of majorite garnet to mag-

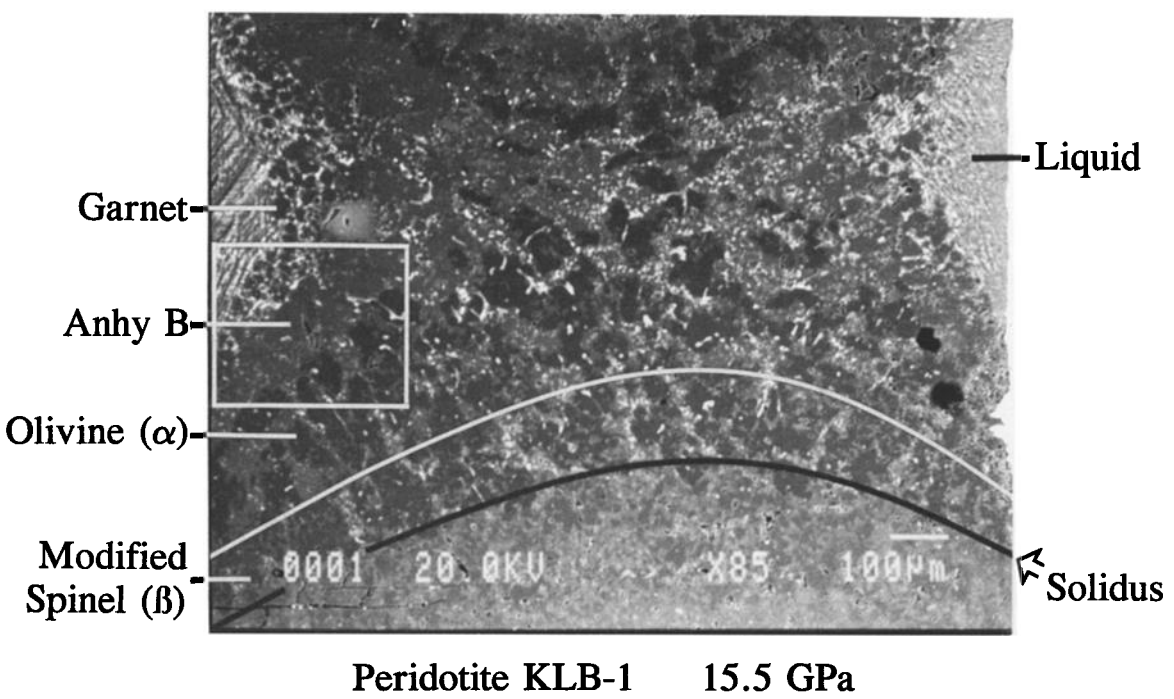

Figure 9. Backscatter SEM photomicrograph of the 15.5-GPa experiment (KLB1-20) run at a nominal temperature of 2135°C for 6 min. The area inside the box is magnified in Figure 10.

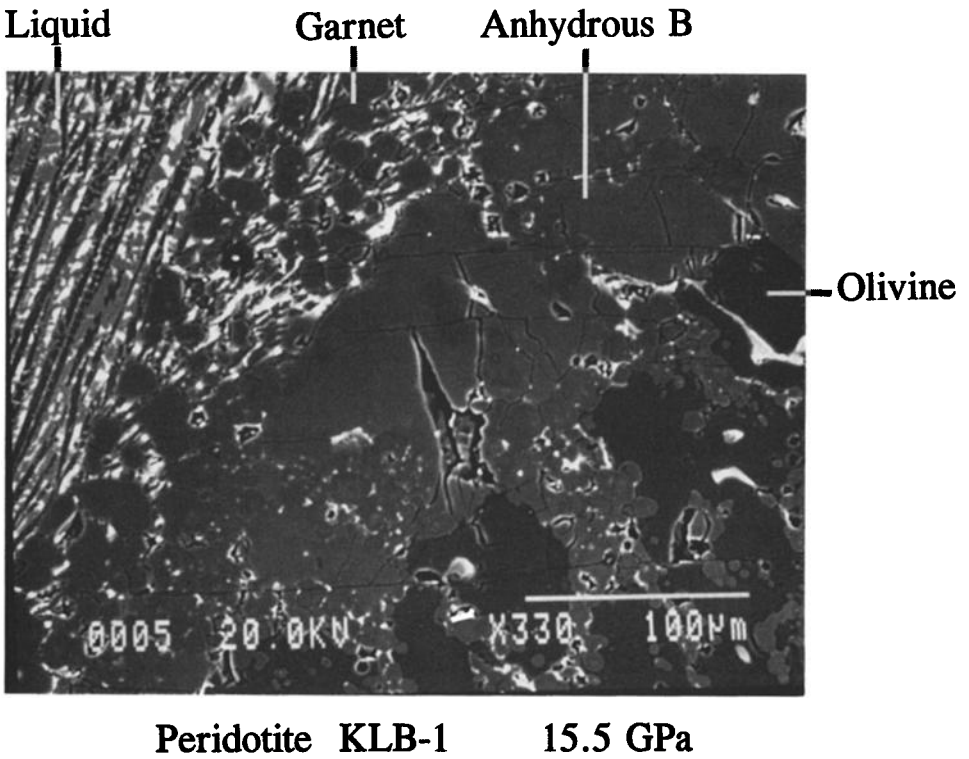

Figure 10. Magnified view of the 15.5-GPa experiment indicated by the box in Figure 9.

nesium silicate perovskite occurs at 22 GPa (Figure 6). This is identical to the transformation in the system $MgSiO_3$ determined in other experiments [*Ito and Katsura*, 1992] and by thermochemical calculation [*Gasparik*, 1990; *Fei et al.*, 1990; *Yusa et al.*, 1993].

We will be reporting in a forthcoming paper a comprehensive database of liquid and crystal analyses for experiments in the 5- to 22.5-GPa range. However, we wish to draw attention to the average of many electron microprobe analyses of the all-liquid portions of several experimental

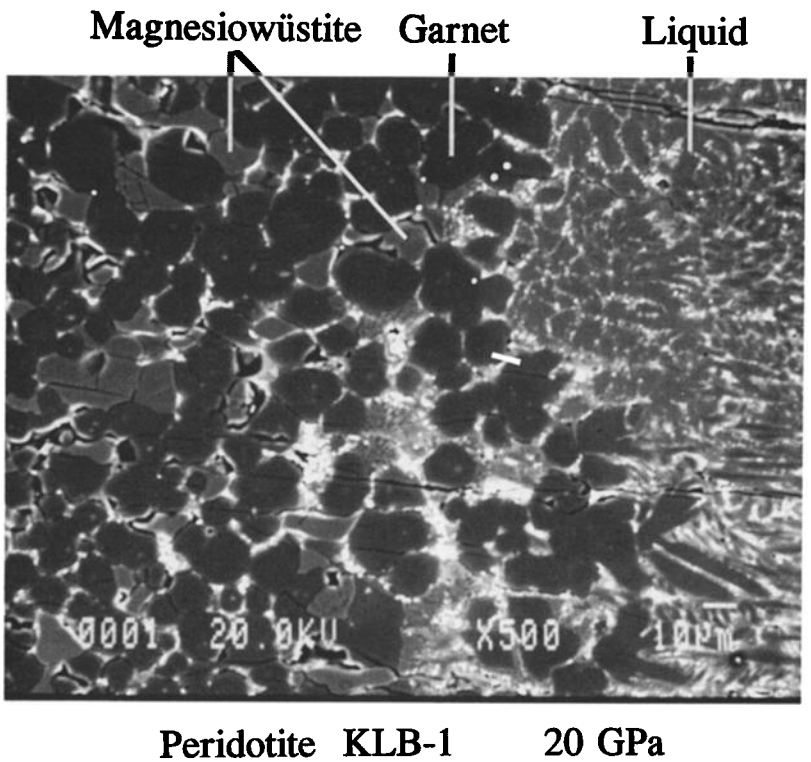

Figure 11. Backscatter SEM photomicrograph of the liquidus portion of a 20-GPa experiment (KLB1-15) run at a nominal temperature of 2215°C.

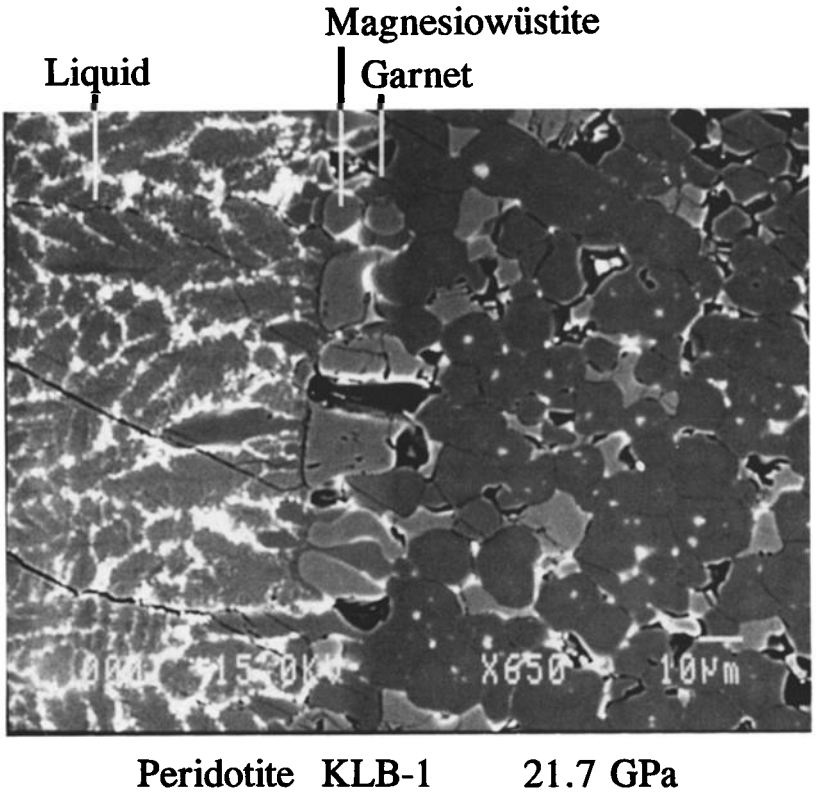

Figure 12. Backscatter SEM photomicrograph of the liquidus portion of an experiment at 21.7 GPa (KLB1-11) run at a nominal temperature of 2240°C and showing multiple saturation in garnet and magnesiowüstite [L + Gt + Mw].

charges (Table 1). It can be seen that the average is similar to the KLB-1 starting material composition, except that it is somewhat lower in MgO; lower MgO is observed also for lower-pressure experiments. This difference arises in part from melt migration but also from the effects of olivine, modified spinel, and magnesiowüstite in removing some MgO during the melting process. The liquidus temperatures and phase equilibria shown in Figure 6 are therefore strictly valid for a peridotite with about 36.6% MgO rather than KLB-1 which contains 39.5% MgO. On the basis of the olivine-liquid thermometer of *Beattie* [1993], the liquidus temperatures shown in Figure 6 will be about 30°C lower than those for KLB-1.

Melting Temperatures

Experimental data that bracket solidus temperatures for the mantle in the garnet peridotite stability field from 2.5 to 5.0 were summarized by *Herzberg* [1983] and *McKenzie and Bickle* [1988], and new data were presented by *Takahashi et al.* [1993]. Our solidus determinations from 5 to 15 GPa (Figure 6) were empirically fitted to these low-pressure data by the equation

$$T\ (°C) = 1002 - 0.96P^2 - 465\ [\ln\ (1/P)]$$

Solidus and liquidus melting temperatures for KLB-1 in this study are compared to those reported by *Takahashi* [1986] and *Takahashi et al.* [1993] in Figure 15. Our melting temperatures at around 15 GPa are about 200°C higher, a difference that arises from different thermocouple configurations in the two studies [*Herzberg et al.*, 1990; *Takahashi et al.*, 1993]. *Takahashi* [1986] adopted a thermocouple which enters the heater through a hole in the side, whereas the one adopted in the present study enters the heater axially. It is most likely that a side-entering thermocouple creates local irregularities in resistance, giving rise to hot spots which are not read by the thermocouple [*Herzberg et al.*, 1990]. The solidus determinations of *Takahashi et al.* [1993] at 3 to 6.5 GPa are in perfect agreement with ours because they adopted an axial thermocouple configuration similar to the one used in this study. More recently, the phase diagram for KLB-1 has been reevaluated by *Shimazaki and Takahashi* [1993], and the solidus temperatures are now in very good agreement over the entire 2.5- to 15.0-GPa range.

A cusp is very prominent in the solidus at 15.5 GPa where olivine transforms into modified spinel and where all clinopyroxene becomes dissolved into garnet (Figure 6). There is a strong change in the slope dT/dP of the solidus at higher pressures, and in the 18- to 22.5-GPa range it appears flat. It is important to note, however, that the phase diagrams for KLB-1 reported here and by *Shimazaki and Takahashi* [1993] have no negative slopes in the melting curves as had been reported earlier [*Takahashi*, 1986].

Discussion of Results

The first liquidus phase diagrams that were experimentally determined for peridotite compositions with the multianvil press [*Takahashi and Scarfe*, 1985; *Takahashi*, 1986; *Ito and Takahashi*, 1987] have been reproduced in a qualitative manner [*Herzberg et al.*, 1990] (see also this work) in that

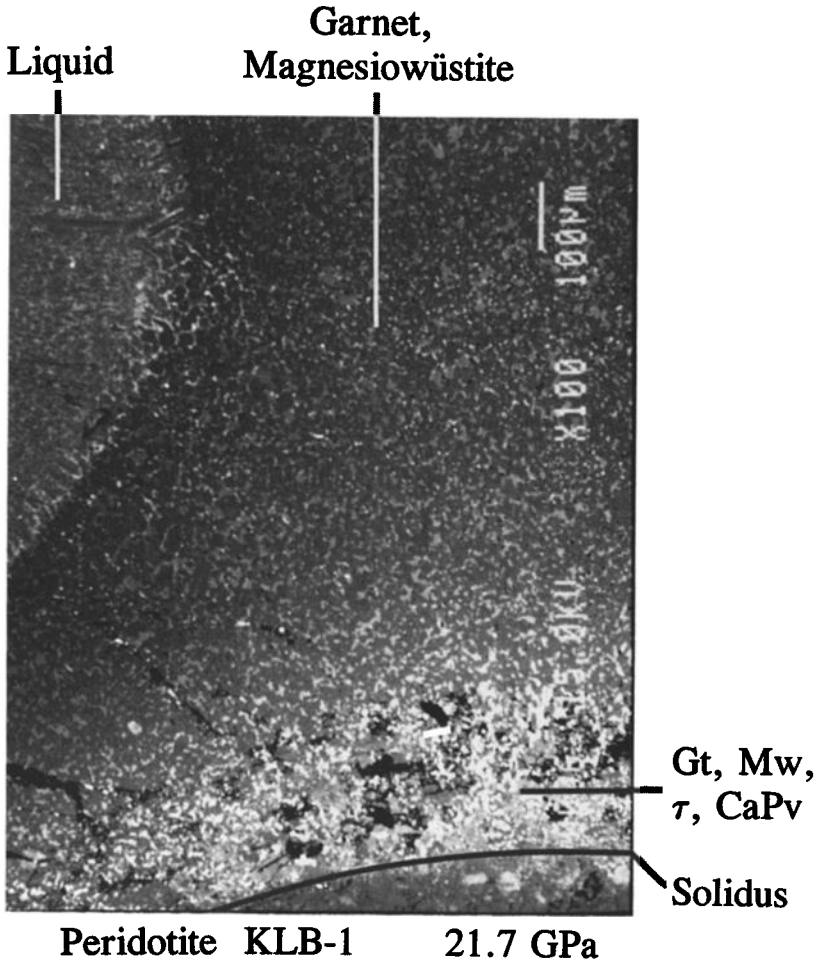

Figure 13. Backscatter SEM photomicrograph of a larger portion of the 21.7-GPa experiment shown in Figure 12.

there is overall agreement in the general topological aspects of the phase diagrams. However, many geological problems require highly precise temperature, pressure, and phase equilibrium information, and it is in the quantitative aspects of the phase diagrams that disagreements have emerged. This problem has been mostly an artifact of differences in experimental method. We are encouraged to see that the most recent phase diagram for KLB-1 reported by *Shimazaki and Takahashi* [1993] is very similar to the one reported here (Figure 6) and that this agreement stems from common experimental methods that were used in the two studies. In particular, use of thermocouples that enter the assembly down the axis of the heater yields temperatures that are remarkably consistent.

Many aspects of the experimental method that have been examined in this paper are supplemental to work that has been reported elsewhere [*Herzberg et al.*, 1990; *Gasparik*, 1989, 1990; *Presnall and Gasparik*, 1990; *Liebermann and Wang*, 1992]. Precision in temperature measurement using W3 %Re versus W25 %Re thermocouples is within ±30°C, and uncertainties stemming from both precision and accuracy may be as good as ±50°C over the entire 5- to 22.5-GPa range. Precision in measurement of pressure with 10-mm assemblies is well within ±0.25 GPa. The oxygen fugacity of 10-mm and 14-mm assemblies that contain peridotite starting material wrapped in unwelded rhenium foil is slightly more oxidizing than the iron-wüstite buffer. The temperature gradient in 14-mm assemblies has been characterized and is so small near the hot spot that melt migration is retarded. Electron probe data, which will be reported in a forthcoming paper, document the extent of melt migration in a temperature gradient for both 10- and 14-mm assemblies. However, triplicate experiments done on KLB-1 at constant temperature and pressure demonstrate that there is no change in the sequence of crystalline phases that appear down the temperature gradient for run durations that span 2 to 12 min in 10-mm assemblies. Chemical equilibrium is reached within 3 min for experiments in the 2000°C range [*Herzberg et al.*, 1990]. Solution and reprecipitation, which are excellent textural criteria for equilibrium, are observed to occur for olivine and garnet crystals.

The new phase diagram for mantle peridotite reported here will be most important for understanding deep melting processes that occur in plumes [*Herzberg*, 1992]. In particular, the solidus temperatures and phase equilibria are essential for understanding how hot the plumes can be and the compositions of komatiites that can form in them. But the phase diagram is also important in addressing a number of theories for the very origin of mantle peridotite. For example, at no pressure do the solidus and liquidus for

mantle peridotite converge to a common temperature or to a narrow range of temperatures. The proposal that there exists compositional identity between mantle peridotite and liquids formed as partial melts [*Herzberg and O'Hara*, 1985] or residual liquids on the solidus is therefore not supported by these experimental results. Although much more work is needed to constrain these compositions, liquids on the solidus in the 5- to 10-GPa range are komatiites with CaO/Al_2O_3 and SiO_2 that are both higher than mantle peridotite [*Herzberg*, 1992]. Preliminary electron probe results indicate that liquids on the solidus at 20 GPa will have CaO/Al_2O_3 in the 2 to 4 range, compared with about 1 for mantle peridotite.

But phase equilibrium control is still indicated for the origin of mantle peridotite because KLB-1 has the properties of a liquid that exhibits cotectic liquidus crystallization behavior involving [L + Gt + Mw] from 18 to 22 GPa. Basalts may provide a possible analog in that many of them owe their geochemical identity to cotectic liquidus crystallization behavior involving [L + Cpx + Plag + Ol] at low pressures [*O'Hara*, 1968; *Walker et al.*, 1979]. Although differences in magma physics can make these phase equilibrium comparisons misleading, it would be very unusual if it was purely by chance that there exists compositional identity between mantle peridotite and high-pressure cotectic liquid compositions. The implication is that mantle peridotite may indeed be the product of a large-scale differentiation event and that MgO/SiO_2 for mantle peridotite may have been phase equilibrium controlled by cotectic crystallization in a magma ocean.

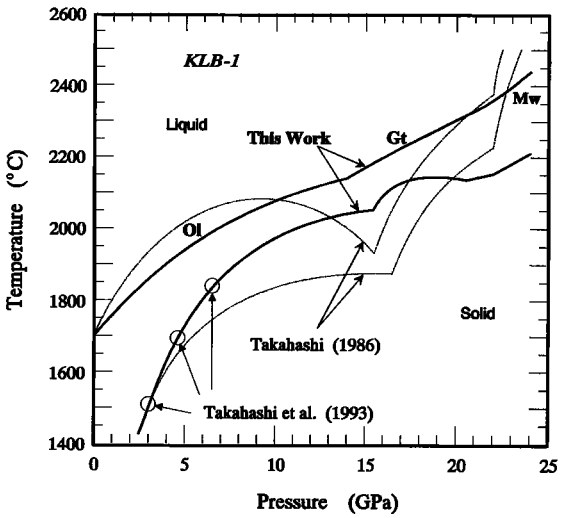

Figure 15. Liquidus and solidus temperatures for anhydrous peridotite KLB-1 reported here (solid lines) and by *Takahashi* [1986] (dashed lines). Solidus temperatures for KLB-1 reported by *Takahashi et al.* [1993] are also shown (circles).

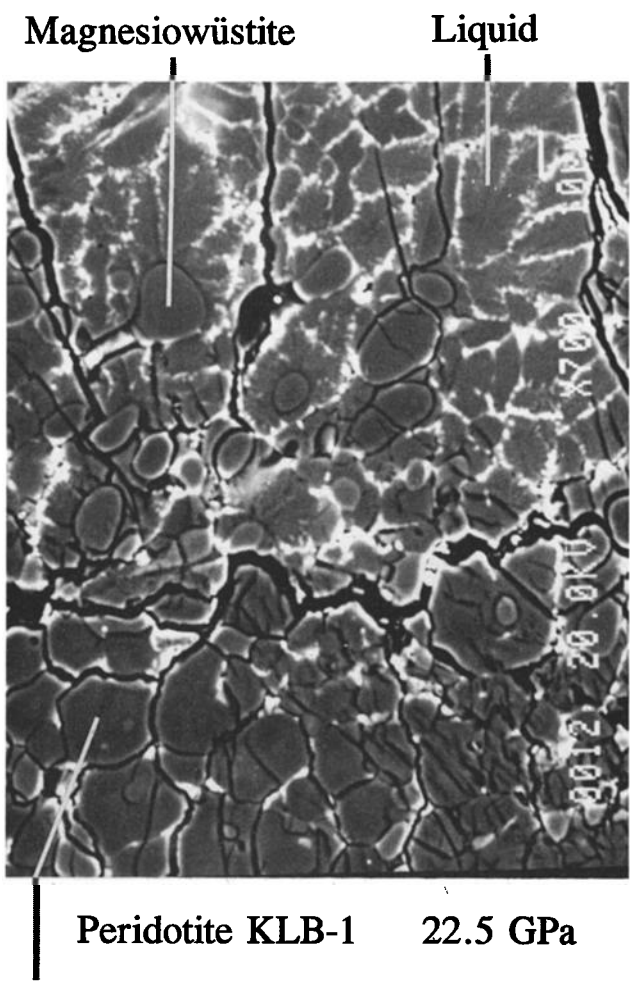

Figure 14. Backscatter SEM photomicrograph of the liquidus portion of a 22.5-GPa experiment (KLB1-36) run at 2375°C. The liquidus follows the isotherm out of the field of view where it terminates next to the thermocouple junction, demonstrating that the nominal temperature equals the liquidus temperature. Magnesiowüstite is the liquidus phase.

A much larger question concerns the distribution of mantle peridotite and the overall MgO/SiO_2 ratio of the Earth, but this is beyond the scope of this paper. It is important to note, however, that our experimental results cannot be used to constrain the MgO/SiO_2 for the bulk Earth. If it is chondritic, then it may be inferred that mantle peridotite formed as a solidified cotectic liquid, and majorite garnet fractionation may have enriched the lower mantle in silica [*Herzberg and Gasparik*, 1991]. Alternatively, if the Earth was made of material in the solar nebula with MgO/SiO_2 that was comparable in composition to mantle peridotite and its pyrolite analog [*McFarlane and Drake*, 1990], then the liquidus phase equilibria reported here may be irrelevant or incidental in understanding Earth structure. An even more intriguing possibility is that the bulk Earth MgO/SiO_2 is greater than that for pyrolite, in which case fractionation of magnesiowüstite to the lower mantle can be inferred from our experimental results. In any case, we end with the cautionary note that MgO/SiO_2 is a property of the Earth that must be measured rather than assumed, and it remains to be determined whether the liquidus phase equilibria reported here are important for understanding Earth structure.

Acknowledgments. This research was partially supported by a grant from the National Science Foundation to C.H. (EAR 91-17184). The high-pressure experiments reported in this paper were performed at the Stony Brook High Pressure Laboratory, which is now part of the NSF Science and Technology Center for High Pressure Research (EAR 89-20239) established at Stony Brook in conjunction with Princeton University and the Geophysical Laboratory of the Carnegie Institute of Washington. Special thanks are extended to Bjorn Mysen for

use of Raman facilities, Connie Bertka for color-coded electron microprobe maps, and Tibor Gasparik for technical assistance and a critical review of this paper. Richard Arculus is thanked for critical comments. Mineral Physics Institute, Department of Earth and Space Sciences, SUNY, Stony Brook, publication 105.

References

Agee, C. B., and D. Walker, Mass balance and phase density constraints on early differentiation of chondritic mantle, *Earth Planet. Sci. Lett.*, *90*, 144–156, 1988.

Beattie, P., Olivine-melt and orthopyroxene-melt equilibria, *Contrib. Mineral. Petrol.*, *115*, 103–111, 1993.

Bertka, C. M., and J. R. Holloway, Pigeonite at solidus temperatures: Implications for partial melting, *J. Geophys. Res.*, *98*, 19,755–19,766, 1993.

Canil, D., Orthopyroxene stability along the peridotite solidus and the origin of cratonic lithosphere beneath southern Africa, *Earth Planet. Sci. Lett.*, *111*, 83–95, 1992.

Davis, B. T. C., The system diopside-forsterite-pyrope at 40 kilobars, *Year Book Carnegie Inst. Washington*, *63*, 165–171, 1964.

Fei, Y., S. K. Saxena, and A. Navrotsky, Internally consistent thermodynamic data and equilibrium phase relations for compounds in the system MgO-SiO_2 at high pressure and high temperature, *J. Geophys. Res.*, *95*, 6915–6928, 1990.

Finger, L. W., J. Ko, R. M. Hazen, T. Gasparik, R. J. Hemley, C. T. Prewitt, and D. J. Weidner, Crystal chemistry of phase B and an anhydrous analogue: Implications for water storage in the upper mantle, *Nature*, *341*, 140–142, 1989.

Gasparik, T., Transformation of enstatite-diopside-jadeite pyroxenes to garnet, *Contrib. Mineral. Petrol.*, *102*, 389–405, 1989.

Gasparik, T., Phase relations in the transition zone, *J. Geophys. Res.*, *95*, 15,751–15,769, 1990.

Herzberg, C. T., Solidus and liquidus temperatures and mineralogies for anhydrous garnet-lherzolite to 15 GPa, *Phys. Earth Planet. Inter.*, *32*, 193–202, 1983.

Herzberg, C., Depth and degree of melting of komatiites, *J. Geophys. Res.*, *97*, 4521–4540, 1992.

Herzberg, C., and T. Gasparik, Garnet and pyroxenes in the mantle: A test of the majorite fractionation hypothesis, *J. Geophys. Res.*, *96*, 16,263–16,274, 1991.

Herzberg, C. T., and M. J. O'Hara, Origin of mantle peridotite and komatiite by partial melting, *Geophys. Res. Lett.*, *12*, 541–544, 1985.

Herzberg, C., T. Gasparik, and H. Sawamoto, Origin of mantle peridotite: Constraints from melting experiments to 16.5 GPa, *J. Geophys. Res.*, *95*, 15,779–15,803, 1990.

Irifune, T., and A. E. Ringwood, Phase transformations in primitive MORB and pyrolite compositions to 25 GPa and some geophysical implications, in *High-Pressure Research in Mineral Physics*, *Geophys. Monogr. Ser.*, vol. 39, edited by M. H. Manghnani and Y. Syono, pp. 231–242, AGU, Washington, D. C., 1987.

Ito, E., and T. Katsura, Melting of ferromagnesian silicates under the lower mantle conditions, in *High-Pressure Research: Application to Earth and Planetary Sciences*, *Geophys. Monogr. Ser.*, vol. 67, edited by Y. Syono and M. H. Manghnani, pp. 315–322, AGU, Washington, D. C., 1992.

Ito, E., and E. Takahashi, Melting of peridotite under the lower mantle condition, *Nature*, *328*, 514–517, 1987.

Ito, E., and E. Takahashi, Postspinel transformations in the system Mg_2SiO_4-Fe_2SiO_4 and some geophysical implications, *J. Geophys. Res.*, *94*, 10,637–10,646, 1989.

Kato, T., and M. Kumazawa, Melting experiment on natural lherzolite at 20 GPa: Formation of phase B coexisting with garnet, *Geophys. Res. Lett.*, *13*, 181–184, 1986.

Kato, T., A. E. Ringwood, and T. Irifune, Experimental determination of element partitioning between silicate perovskites, garnets and liquids: Constraints on early differentiation of the mantle, *Earth Planet. Sci. Lett.*, *89*, 123–145, 1988a.

Kato, T., A. E. Ringwood, and T. Irifune, Constraints on element partition coefficients between $MgSiO_3$ perovskite and liquid determined by direct measurements, *Earth Planet. Sci. Lett.*, *90*, 65–68, 1988b.

Katsura, T., and E. Ito, The system Mg_2SiO_4-Fe_2SiO_4 at high pressures and temperatures: Precise determination of stabilities of olivine, modified spinel, and spinel, *J. Geophys. Res.*, *94*, 15,663–15,670, 1989.

Lesher, C. E., and D. Walker, Cumulate maturation and melt migration in a temperature gradient, *J. Geophys. Res.*, *93*, 10,295–10,311, 1988.

Liebermann, R. C., and Y. Wang, Characterization of sample environment in a uniaxial split-sphere apparatus, in *High-Pressure Research: Application to Earth and Planetary Sciences*, *Geophys. Monogr. Ser.*, vol. 67, edited by Y. Syono and M. H. Manghnani, pp. 19–31, AGU, Washington, D. C., 1992.

McFarlane, E. A., and M. J. Drake, Element partitioning and the early thermal history of the Earth, in *Origin of the Earth*, edited by H. E. Newsom and J. H. Jones, pp. 135–150, Oxford University Press, New York, 1990.

McFarlane, E. A., M. J. Drake, and C. T. Herzberg, Magnesiowüstite/melt and majorite/melt partitioning and the early thermal history of the Earth (abstract), *Proc. Lunar Planet. Sci. Conf.*, *22*, 875–876, 1991.

McKenzie, D., and M. J. Bickle, The volume and composition of melt generated by extension of the lithosphere, *J. Petrol.*, *29*, 625–679, 1988.

McMillan, P., and M. Akaogi, Raman spectra of β-Mg_2SiO_4 (modified spinel) and γ-Mg_2SiO_4 (spinel), *Am. Mineral.*, *72*, 361–364, 1987.

Mirwald, P. W., and H.-J. Massonne, The low-high quartz and quartz-coesite transition to 40 kbar between 600 and 1600°C and some reconnaissance data on the effect of $NaAlO_2$ component on the low quartz-coesite transition, *J. Geophys. Res.*, *85*, 6983–6990, 1980.

O'Hara, M. J., Are ocean floor basalts primary magmas?, *Nature*, *220*, 683–686, 1968.

O'Hara, M. J., and H. S. Yoder, Jr., Formation and fractionation of basic magmas at high pressures, *Scott. J. Geol.*, *3*, 67–117, 1967.

Presnall, D. C., and T. Gasparik, Melting of enstatite ($MgSiO_3$) from 10 to 16.5 GPa and the forsterite (Mg_2SiO_4)–majorite ($MgSiO_3$) eutectic at 16.5 GPa: Implications for the origin of the mantle, *J. Geophys. Res.*, *95*, 15,771–15,778, 1990.

Presnall, D. C., and M. J. Walter, Melting of forsterite, Mg_2SiO_4, from 9.7 to 16.5 GPa, *J. Geophys. Res.*, *98*, 19,777–19,783, 1993.

Shimazaki, T., and E. Takahashi, High-pressure melting of a peridotite KLB-1: On the early melting history of the Earth, *Eos Trans. AGU*, *74*(43), Fall Meeting suppl., 655, 1993.

Susaki, J., M. Akaogi, S. Akimoto, and O. Shimomura, Garnet-perovskite transformation in $CaGeO_3$: In-situ X-ray measurements using synchrotron radiation, *Geophys. Res. Lett.*, *12*, 729–732, 1985.

Takahashi, E., Melting of a dry peridotite KLB-1 up to 14 GPa: Implications on the origin of peridotitic upper mantle, *J. Geophys. Res.*, *91*, 9367–9382, 1986.

Takahashi, E., and C. M. Scarfe, Melting of peridotite to 14 GPa and the genesis of komatiite, *Nature*, *315*, 566–568, 1985.

Takahashi, E., T. Shimazaki, Y. Tsuzaki, and H. Yoshida, Melting study of a peridotite KLB-1 to 6.5 GPa, and the origin of basaltic magmas, *Philos. Trans. R. Soc. London, A*, *342*, 105–120, 1993.

Walker, D., and C. Agee, Partitioning "equilibrium," temperature gradients, and constraints on Earth differentiation, *Earth Planet. Sci. Lett.*, *96*, 49–60, 1989.

Walker, D., T. Shibata, and S. E. DeLong, Abyssal tholeiites from the oceanographer fracture zone, II, Phase equilibria and mixing, *Contrib. Mineral. Petrol.*, *70*, 111–125, 1979.

Yusa, H., M. Akaogi, and E. Ito, Calorimetric study of $MgSiO_3$ garnet and pyroxene: Heat capacities, transition enthalpies, and equilibrium phase relations in $MgSiO_3$ at high pressures and temperatures, *J. Geophys. Res.*, *98*, 6453–6460, 1993.

Zerr, A., and R. Boehler, Melting of (Mg, Fe)SiO_3-perovskite to 625 kilobars: Indication of a high melting temperature in the lower mantle, *Science*, *262*, 553–555, 1993.

Zhang, J., R. C. Liebermann, T. Gasparik, C. T. Herzberg, and Y. Fei, Melting and subsolidus relations of SiO_2 at 9 to 14 GPa, *J. Geophys. Res.*, *98*, 19,785–19,793, 1993.

C. Herzberg, Department of Geological Sciences, Rutgers University, Piscataway, NJ 08855-1179.

J. Zhang, Center for High Pressure Research and Mineral Physics Institute, The State University of New York at Stony Brook, Stony Brook, NY 11794.

(Received October 19, 1993; revised April 8, 1994;
accepted May 18, 1994.)